January 1, 2018

Structural and Functional Brain Imaging in Acute HIV

Vishal Samboju, *University of California, San Francisco*
Carissa L. Philippi, *University of Missouri–St. Louis*
Phillip Chan, *SEARCH, Thai Red Cross AIDS Research Centre, Bangkok, Thailand*
Yann Cobigo, *University of California, San Francisco*
James L.K. Fletcher, *SEARCH, Thai Red Cross AIDS Research Centre, Bangkok, Thailand*, et al.

NeuroImage: Clinical 20 (2018) 327–335

Contents lists available at ScienceDirect

NeuroImage: Clinical

journal homepage: www.elsevier.com/locate/ynicl

Structural and functional brain imaging in acute HIV

Vishal Samboju[a,1], Carissa L. Philippi[b,1], Phillip Chan[c], Yann Cobigo[a], James L.K. Fletcher[c], Merlin Robb[d,e], Joanna Hellmuth[a], Khunthalee Benjapornpong[c], Netsiri Dumrongpisutikul[f], Mantana Pothisri[f], Robert Paul[b], Jintanat Ananworanich[c,d,e,g], Serena Spudich[h], Victor Valcour[a,*], for the , SEARCH 010/RV254, RV304 protocol teams

[a] Memory and Aging Center, Department of Neurology, University of California, San Francisco, CA, USA
[b] University of Missouri St. Louis, Department of Psychological Sciences, St. Louis, MO, USA
[c] SEARCH, Thai Red Cross AIDS Research Centre, Bangkok, Thailand
[d] U.S. Military HIV Research Program, Walter Reed Army Institute of Research, Silver Spring, MD, USA
[e] Henry M. Jackson Foundation for the Advancement of Military Medicine, Bethesda, MD, USA
[f] Department of Radiology, Chulalongkorn University Medical Center, Bangkok, Thailand
[g] Department of Global Health, The University of Amsterdam, Amsterdam, The Netherlands
[h] Department of Neurology, Yale University, New Haven, CT, USA

A B S T R A C T

Background: HIV RNA is identified in cerebrospinal fluid (CSF) within eight days of estimated viral exposure. Neurological findings and impaired neuropsychological testing performance are documented in a subset of individuals with acute HIV infection (AHI). The purpose of this study was to determine whether microstructural white matter and resting-state functional connectivity (rsFC) are disrupted in AHI.

Methods: We examined 49 AHI (100% male; mean age = 30 ± SD 9.9) and 23 HIV-uninfected Thai participants (78% male; age = 30 ± 5.5) with diffusion tensor imaging (DTI) and rsFC acquired at 3 Tesla, and four neuropsychological tests (summarized as NPZ-4). MRI for the AHI group was performed prior to combination antiretroviral treatment (ART) in 26 participants and on average two days (range:1–5) after ART in 23 participants. Fractional anisotropy (FA), mean (MD), axial (AD), and radial diffusivity (RD) were quantified for DTI. Seed-based voxelwise rsFC analyses were completed for the default mode (DMN), fronto-parietal, and salience and 6 subcortical networks. rsFC and DTI analyses were corrected for family-wise error, with voxelwise comparisons completed using *t*-tests. Group-specific voxelwise regressions were conducted to examine relationships between imaging indices, HIV disease variables, and treatment status.

Results: The AHI group had a mean (SD) CD4 count of 421(234) cells/mm^3 plasma HIV RNA of 6.07(1.1) $\log_{10}$ copies/mL and estimated duration of infection of 20(5.5) days. Differences between AHI and CO groups did not meet statistical significance for DTI metrics. Within the AHI group, voxelwise analyses revealed associations between brief exposure to ART and higher FA and lower RD and MD bilaterally in the corpus callosum, corona radiata, and superior longitudinal fasciculus ($p < 0.05$). Diffusion indices were unrelated to clinical variables or NPZ-4. The AHI group had reduced rsFC between left parahippocampal cortex (PHC) of the DMN and left middle frontal gyrus compared to CO ($p < 0.002$). Within AHI, ART status was unrelated to rsFC. However, higher CD4 cell count associated with increased rsFC for the right lateral parietal and PHC seeds in the DMN. Direct associations were noted between NPZ-4 correspond to higher rsFC of the bilateral caudate seed ($p < 0.002$).

Conclusions: Study findings reveal minimal disruption to structural and functional brain integrity in the earliest stages of HIV. Longitudinal studies are needed to determine if treatment with ART initiated in AHI is sufficient to prevent the evolution of brain dysfunction identified in chronically infected individuals.

1. Introduction

HIV is known to impact the central nervous system (CNS) and result in functional and neuropsychological impairment that underlie HIV-associated neurocognitive disorder (HAND) (Heaton et al., 2004). While the introduction of antiretroviral therapy (ART) has decreased the frequency of more severe forms of HAND, the overall prevalence remains unchanged at 30–50% among populations with access to ART (Heaton et al., 2010). Structural and functional brain abnormalities have been reported in later stages of HIV infection; yet, it remains unknown when in the course of HIV infection these structural or functional CNS changes occur (O'Connor et al., 2018; Hakkers et al., 2017). Acute HIV infection (AHI), the first weeks following infection when HIV antibody is often undetectable, is the earliest stage of the

* Corresponding author.
E-mail address: Victor.Valcour@ucsf.edu (V. Valcour).
[1] Co-first authors.

https://doi.org/10.1016/j.nicl.2018.07.024
Received 21 March 2018; Received in revised form 30 June 2018; Accepted 25 July 2018
Available online 27 July 2018

disease and is distinguished from individuals identified during early or primary HIV (< 1 year of infection) and chronic HIV infection (> 1 year after infection) (Fiebig et al., 2003). In chronic HIV, people with HAND can experience worse performance in executive, attention, working memory, and information processing speed (Woods et al., 2009). Structural brain changes may underlie these cognitive issues, as white and gray matter differences have been seen in older age in fully suppressed chronically infected HIV participants using diffusion tensor imaging (DTI) and volumetric measurements (Underwood et al., 2017; Stebbins et al., 2007; Su et al., 2016; Jernigan et al., 2011; Ances et al., 2012). AHI is also marked by very high plasma viremia, which, when untreated contributes to the morbidity and mortality of HIV and to HIV associated dementia in the chronic phase of disease (Price & Spudich, 2008; Lavreys et al., 2006; Watkins & Treisman, 2015; Sidtis et al., 1993). However, initiation of ART during AHI precedes establishment of viral set-point and lowers viral reservoir levels in peripheral blood mononuclear cells, potentially altering disease trajectory (Ananworanich et al., 2016). Examining early structural and functional alterations in the brain during AHI allows us to understand if early treatment can mitigate changes that result in cognitive impairment in later stages and provides critical knowledge regarding the initial CNS sites of infection that are involved.

Neuropsychological testing abnormalities and neurological exam findings are present in some individuals during AHI, and may be caused by structural brain changes. HIV RNA is detected in the cerebrospinal fluid (CSF) as early as eight days after estimated exposure to HIV, although gross widespread structural CNS differences have not been identified in AHI (Kore et al., 2015; Hellmuth et al., 2016; Valcour et al., 2012; Ragin et al., 2015; Filippi et al., 2001). Standard volumetric techniques explored to date are less sensitive and may not detect changes in this early phase, as Magnetic Resonance Spectroscopy (MRS) suggests cellular inflammation is present in AHI (Sailasuta et al., 2012). Identifying vulnerable neuroanatomy through more sensitive neuroimaging techniques will inform whether microstructural damage exists and could support the identification of initial CNS sites involved.

Few studies have examined neuroanatomical changes occurring during AHI using DTI and resting-state functional magnetic resonance imaging (rs-fMRI). Cao et al. reported reduced regional brain volumes and white matter microstructural neuroimaging abnormalities in a small sample of individuals with HIV disease duration of 0–4 months (Cao et al., 2015). However, the group reported high rates of illicit substance use and mixed ART status. Separate analyses of the same cohort revealed brainstem and third ventricular enlargement in conjunction with parenchymal reduction and reduced microstructural integrity of the white matter quantified by DTI (Ragin et al., 2015). Brain volumes also correlated with cytokine levels (Ragin et al., 2015). This study also postulated engagement of the corpus callosum as the primary site of viral brain infiltration by documenting comparatively lower white matter integrity quantified using DTI compared to controls. Another study detected diminished resting-state functional connectivity (rsFC) of the inferior parietal cortex within the lateral occipital network in primary HIV infection, within 1 year of infection (7 out of 15 were treatment naïve), as compared with controls (Wang et al., 2011). In this study, rsFC within the lateral occipital network was correlated with neuropsychological performance among those with HIV (Wang et al., 2011).

Together, these data suggest that DTI and rs-fMRI may be useful in detecting early alterations in brain structure and function in AHI. Here, we utilize DTI and rs-fMRI to compare 49 AHI participants to 23 demographically similar, uninfected controls to determine whether microstructural white matter and rsFC of cortical and subcortical networks are disrupted during AHI. We examined relationships between both white matter integrity and rsFC and immune system function (CD4:CD8 ratios), viral load (HIV RNA), and cognitive performance (NPZ-4).

2. Methods

2.1. Participant selection

We enrolled participants seeking HIV testing who were determined to be in AHI at the Anonymous clinic of the Thai Red Cross AIDS Research center in Bangkok, Thailand. Most were classified in the primary Fiebig stages of AHI: Fiebig stage I (HIV RNA+, p24 antigen-, HIV IgM-, n = 3), stage II (HIV RNA+, p24 antigen+, HIV IgM-, n = 10), stage III (HIV IgM+, Western Blot -, n = 30), stage IV (HIV IgM+, Western Blot indeterminate, (n = 4)), stage V (Western Blot+ without p31 band, n = 2) and agreed to imaging, laboratory assessments, and clinical follow-up as outlined in a broader protocol set to investigate the immunology and virology of AHI (SEARCH 010/RV 254, ClinicalTrials.gov identifier NCT00796146) (Fiebig et al., 2003; De Souza et al., 2015). Infection duration was calculated by participant's self-reported exposure date, or by taking the median date of multiple potential exposures.

In this study, we compare AHI participants (n = 49) with demographically similar, age matched HIV uninfected controls (n = 23) enrolled from concurrent HIV protocols (RV304/SEARCH 013: NCT01397669). Any AHI participants showing positive serology for syphilis (serum VDRL) at diagnosis were excluded (n = 10). We examined all SEARCH 010/RV254 participants who consented to and underwent neuroimaging on a 3.0 Tesla MRI (dates: 7/6/2015–3/14/2017) were chosen from the greater population of those enrolling in the protocol. All control participants were scanned on the same MRI with identical scanning sequences and parameters. Of the 69 AHI eligible participants, full data were available for 49, after excluding participants due to positive serum syphilis serology (n = 10), and excessive motion during resting-state (n = 7) and DTI (n = 3) scans.

Among a broader set of clinical and laboratory variables captured at baseline, this analysis utilized a four test neuropsychological battery (NPZ-4), CD4 lymphocyte counts, CD8 lymphocyte counts, and plasma HIV RNA (copies/mL). MRI for the AHI group was performed *prior* to combination ART in 26 participants, and a mean (SD) of 2(1.1) days *after* combination ART initiation in 23 participants. The study was approved by institutional review boards from all participating sites all participants also provided written and informed consent.

2.2. Neuropsychological assessment

Our four-category neuropsychological testing battery included of the Grooved Pegboard test non-dominant hand (fine motor function), Color trails 1 (psychomotor speed), Color Trails 2 (executive functioning/set-shifting) and Trail Making A (psychomotor speed). These tests were combined into an overall cognitive performance score (NPZ-4) conducted and tabulated as previously described (Hellmuth et al., 2016).

2.3. HIV disease variables

Quantification of HIV RNA followed standard measures derived from previous work (De Souza et al., 2015). Corresponding plasma HIV RNA, CD4, and CD8 cell counts were measured the day of enrollment into the study and within a mean (SD) 2.6 (Underwood et al., 2017) days of MRI acquisition. Estimated infection duration was calculated using a median of participants' self-reported exposure date(s), as previously described (Valcour et al., 2012).

2.4. Imaging data acquisition

All structural and functional magnetic resonance imaging (MRI) data were acquired using the same Philips Ingenia 3T MRI scanner equipped with

a 15-channel volume head coil for signal excitation and reception. High-resolution T1-weighted structural images were acquired using a standard T1-weighted imaging turbo field echo (T1W 3D TFE) scan (TR/TE/flip angle (FA): 8.1 ms/3.7 ms/8°, matrix:256 × 256 × 165, field of view (FOV): 256 mm × 256 mm, voxel size: 1 mm × 1 mm × 1 mm, number of slices: 165, no gap). DTI and rsFC scans were all captured on the same version and hardware. DTI sequences included gradients applied in 32 directions with a b value of 1000 s/mm^2 (TR/TE/FA: 11000 ms/111 ms/90°, matrix size = 128 × 126, FOV: 256 mm × 256 mm and slice thickness: 2 mm × 2 mm × 2 mm, number of slices: 2380 axial; slices). Resting-state functional images were acquired using T2*-weighted Echo Planar Imaging (EPI) sequence (TR/TE/FA: 1600 ms/22 ms/70°, matrix size: 128 × 128, FOV: 224 mm × 224 mm slice thickness: 1.75 mm × 1.75 mm × 3.5 mm, number of slices: 9694 axial slices) for the resting-state scan acquired with the subject's eyes closed (lasting about ~7 min/262 volumes).

2.5. Preprocessing and template creation for DTI

We applied the FSL MCFLIRT algorithm to register DWI images to the primary volume of the sequence (Jenkinson et al., 2002). Data reflecting absolute displacement parameters beyond 1 mm were screened out and volumes surpassing relative displacement parameters beyond 1 mm were removed (n = 3). Background voxels not considered as brain tissue were then masked out of the DWI volumes by applying a median otsu function (Garyfallidis et al., 2014). This function utilized the B_0 acquisitions to provide a mask using otsu thresholding with a 4 mm radius and 4 iterations to minimize intra-class variance (Garyfallidis et al., 2014). We used the re-aligned diffusion images, the mask, and the b-vectors and b-values to correct for eddy current-induced distortions (FSL Eddy). Remaining tensors were then fitted using DIPY with a non-linear least-squares approach derived fitting model to construct FA, MD, RD and AD maps from standard equations (Garyfallidis et al., 2014; Pierpaoli & Basser, 1996).

Post processing steps included construction of a group template and normalization of DTI metric maps into standard DTI-TK space for Tensor Based Registration (Zhang et al., 2007a,b). A Thai group template was created using tensor based registration of participants' processed DTI volumes through a boot strapping algorithm to a standard DTI template provided by DTI-TK. The next step involved computing affine alignment transformations using DTI-TK (dti_affine_population) to place all participants into standard space employing a normalized mutual information cost function with 3 iterations. A binary mask was then created using (BinaryThresholdImageFilter) the trace diffusion (MD) map to mask out tensors outside template brain tissue. A final deformable alignment (dti_diffeomorphic_population) was then used to register all participants to iteratively refine the Thai template. The stored affine transformations and displacement field vectors are then computed to a combined displacement field (dfRightComposeAffine) and applied (deformationSymTensor3DVolume) to transform the native participant DTI volumes to standard Thai template space to minimize interpolation steps.

2.6. Diffusion indices analysis

Analyses followed conventional tract based spatial statistics (TBSS) integration pipeline using DTI-TK. After the post processing steps were completed, proceeding skeleton creation, projection and statistics were carried out using standard FSL TBSS processing (FMRIB Software Library; http://fsl.fmrib.ox.ac.uk/fsl/fslwiki/TBSS). A white matter skeleton was created from FA maps to enhance statistical comparison of peak white matter tracts based on previous work by Smith et al. (2006).

Region of interest analyses were conducted by masking different ROIs derived from the Johns Hopkins atlas onto diffusion index maps (FA, MD, RD, and AD) for each participant. We accomplished this by estimating (fsl_reg) and applying (applywarp) warping parameters to transform the Johns Hopkins University atlas (JHU) space to the DTI-TK space template. Mean DTI metrics were then extracted using ANTs (ImageIntensityStatistics) for ROIs of interest chosen based on existing literature. The ROIs included: the corpus callosum identified as having lower FA values in early infection, corona radiata affected in early and chronic HIV, and superior longitudinal fasciculus considered an affected and sensitive tract in early HIV were included (Ragin et al., 2015; Wendelken et al., 2016; Gongvatana et al., 2009).

2.7. Preprocessing and motion analysis for resting-state fMRI data

2.7.1. Preprocessing steps

The resting-state functional data were processed in AFNI and FSL (FMRIB Software Library; http://fsl.fmrib.ox.ac.uk/fsl/fslwiki/) (Cox, 1996). First, the following preprocessing steps were performed (Heaton et al., 2004): images were deobliqued (3dWarp) (Heaton et al., 2010), first three volumes were omitted (3dcalc) (O'Connor et al., 2018), motion corrected by rigid body alignment to the first EPI acquisition (3dvolreg) (Hakkers et al., 2017), the 3D + time series were despiked to remove time series outliers (3dDespike), and (Fiebig et al., 2003) temporally filtered (band-pass: 0.009 Hz < f < 0.08 Hz; 3dTproject) and spatially smoothed with a 3D 4-mm full-width half-maximum (FWHM) Gaussian kernel (3dmerge). Next, the skull-stripped anatomical scan for each participant was rigidly coregistered first with the T1, then with the EPI, and diffeomorphically aligned to Montreal Neurological Institute (MNI)-152 template space using a symmetric normalization algorithm (Zhang et al., 2007a). Normalized T1 anatomical images (i.e., aligned to the EPI and in original space) were also segmented into gray matter, white matter, and CSF using FAST in FSL (Zhang et al., 2001). White matter and CSF segments were used as masks to extract a representative time series from each tissue type. A whole-brain mask was used to extract the time series for the global signal. Final preprocessing steps were performed in a GLM (3dDeconvolve) to account for motion and other typical nuisance variables (Heaton et al., 2004, 2010; O'Connor et al., 2018; Hakkers et al., 2017; Fiebig et al., 2003; Woods et al., 2009): six motion parameters (three translations, three rotations) obtained from the rigid body alignment of EPI volumes and their six derivatives (Underwood et al., 2017), the white matter time series and the derivative (Stebbins et al., 2007), the ventricular (CSF) time series and the derivative, and (Su et al., 2016) a whole-brain or global signal time series and the derivative (Ciric et al., 2017). To further control for individual motion within the GLM, volumes were censored for excessive motion, as described below (i.e., framewise motion displacement and extreme timeseries displacement; see “Motion analysis”). The resulting preprocessed resting-state data was used in the functional connectivity analysis described below.

2.7.2. Motion analysis

We also examined motion for each participant, as individual differences in participant motion can contribute to resting-state correlations (Power et al., 2012). Seven participants (6AHI: 1 control) were excluded due to excessive motion based on the following criteria: mean framewise motion displacement (i.e., volume to volume movement across the time series) > 3 mm, and/or total scan time < 3 min after censoring all time points with framewise motion displacement > 0.2 mm and extreme timeseries displacement (i.e., time points where > 10% of voxels were outliers) (Power et al., 2012). The number of participants excluded due to motion according to HIV group was as follows: AHI Group (Woods et al., 2009); HIV uninfected Group (Heaton et al., 2004). These specific thresholds were selected based on previous research to provide the most conservative criteria for motion correction (Power et al., 2014; Satterthwaite et al., 2013; Yan et al., 2013). As in previous work, average relative root-mean-squared (RMS) displacement was used as a summary measure of participant motion (Ciric et al., 2017). Importantly, using this summary measure, there were no significant differences in average RMS motion between the AHI and HIV uninfected groups (t (70) = 0.20, p > 0.80) were observed.

2.8. Functional connectivity analysis

We performed seed-based voxelwise functional connectivity analyses for 21 seed regions of interest (ROIs) for 3 cortical networks [default mode (DMN), frontoparietal (FPN), and cingulo-opercular (CON)] and 6 subcortical striatal networks [dorsal caudate (DC), dorsal caudal putamen (DCP), dorsal rostral putamen (DRP), ventral rostral putamen (VRP), ventral striatum inferior (VSi), ventral striatum superior (VSs)] (Table 2, Supplementary Fig. 1) (Andrews-Hanna et al., 2010; Di Martino et al., 2008; Biswal et al., 1995). These network seed ROIs were selected as they have been previously implicated in HIV (Wang et al., 2011; Ipser et al., 2015; Ortega et al., 2015; Thomas et al., 2013; Zhuang et al., 2017; Thomas et al., 2015). All network seed ROIs were generated using the Wake Forest University PickAtlas, to create a spherical seed (6-mm radius for cortical, 4-mm for subcortical) centered on the coordinates for each ROI in MNI space (Maldjian et al., 2003). The transformation matrix from the registration procedure described above was used to transform each seed from MNI space to original space (3dfractionize), with the accuracy of seed locations for each participant verified by one of the authors (C.L.P).

For each participant, the mean resting-state BOLD time series from each seed ROI was included in a GLM (3dDeconvolve). To create the correlation maps for each seed ROI, we performed the following steps (Heaton et al., 2004): used the output from the GLM to convert R^2 values to correlation coefficients (r), and (Heaton et al., 2010) converted the correlation coefficients to z-scores via Fisher's r-to-z transform (as in Philippi et al., 2015). The transformation matrix from the registration procedure described above (see “Preprocessing Steps”) was also used to align the correlation maps for each participant to MNI-152 space. The resulting z-score maps were then entered into the second level statistical analyses.

2.9. Statistical analysis

2.9.1. DTI indices analyses

To examine group differences between AHI and CO, tract based spatial statistics (TBSS) were employed to constrain statistical analysis to voxels defined as having peak values in white matter tracts using a skeletonization procedure (Smith et al., 2006). Family wise error (FWE) error corrected threshold free cluster enhancement (TFCE) using FMRIB Software Library (FSL). Randomise with 5000 permutations at an alpha of 0.05 was used to define significant areas at the whole-brain level (Winkler et al., 2014).

For the region of interest analyses, we used regions outlined in existing literature to inform areas affected in AHI (Ragin et al., 2015). Utilizing the Johns Hopkins DTI white matter atlas we included the corpus callosum (whole and by segment: body, splenium, genu), superior longitudinal fasciculus, and corona radiata. Paired t-tests were used to compare ROIs between AHI and uninfected controls as well as within AHI between the ART exposed group and those receiving ART after imaging.

General linear models were carried out using Stata v13.1 to determine associations between DTI metrics and disease status, NPZ-4, HIV RNA, CD4 cell counts, CD8 cell counts, and CD4:CD8 ratios within the AHI group. Supplementary analyses compared Fiebig groups I and II (n = 13) to later Fiebig stages (n = 36) in ROI analyses using t-tests and voxelwise analyses using voxelwise t-tests with the same parameters as the groupwise HIV status comparisons above.

2.10. rsFC

2.10.1. Functional connectivity analyses

To investigate group differences in cortical and subcortical network rsFC between AHI and HIV uninfected groups, we performed unpaired two-sample t-tests on the z-score connectivity maps derived from the seed-based connectivity analyses for each seed ROI. Similar to the DTI analyses, we also performed voxelwise regression analyses within the AHI group to examine differences in rsFC due to brief exposure to ART, defined as brief exposure versus no exposure to ART. As a follow-up analysis, we also explored differences in rsFC within the AHI group associated with early (stages I and II, n = 13) versus later Fiebig stages using unpaired two-sample t-tests on the z-score connectivity maps derived from the seed-based connectivity analyses for each seed ROI.

To correct for multiple comparisons, we implemented a family-wise error (FWE) correction approach at the cluster level using a whole-brain mask (3dClustSim in AFNI version updated July 2017) and applied cluster-extent thresholding (Carp et al., 2012; Forman et al., 1995). To address the non-Gaussian nature of fMRI data the autocorrelation function (−acf) was used to calculate the FWHM for each participant (3dFWHMx in AFNI) (Eklund et al., 2016). The cluster-extent threshold corresponded to the statistical probability ($\alpha = 0.05$, or 5% chance) of identifying a random noise cluster at a predefined voxelwise threshold of $p < 0.001$ (uncorrected). In the present study, using this whole-brain FWE cluster correction and Bonferroni correction for the number of seed ROIs (n = 21), a cluster-corrected size of ≥163 voxels was significant at $p_{FWE} < 0.002$ (0.05/21 = 0.002) in the group analyses reported below. These results were overlaid on the normalized mean anatomical image.

We also performed separate voxelwise regression analyses (3dttest ++ in AFNI) within the AHI group to examine the relationship between rsFC and NPZ-4 and clinical variables (HIV RNA, CD4 cell counts, CD8 cell counts, and CD4:CD8 ratios).

3. Results

The 49 AHI participants did not differ from control participants in terms of age or education ($p > 0.05$), however there were proportionally more females in the control group ($p < 0.001$) Table 1. The AHI group had a mean (SD) CD4 count of 421(234) cells/mm^3 plasma HIV RNA of 6.07(1.1) $\log_{10}$ copies/mL and estimated duration of infection of 20(5.5) days. Most AHI participants were classified into primary Fiebig stages I (6%), II (20%), and III (61%) with 46 (86%) participants showing signs of acute retroviral syndrome defined by a

Table 1
Participant demographics and baseline information.

	AHI participants	HIV uninfected	p-value
Number of participants	49	23	
Age, Mean(SD)	30(9.9)	30(5.5)	0.862
Sex male/female	49/0	18/5	< 0.001
Education (% with bachelor's degree)	55%	39%	0.208
Estimated days of infection, Mean(SD)	20(5.5)	–	–
Fiebig stage I, n(%)	3(6)	–	–
Fiebig stage II, n(%)	10(20)	–	–
Fiebig stage III, n(%)	30(61)	–	–
Fiebig stage IV, n(%)	4(8)	–	–
Fiebig stage V, n(%)	2(4)	–	–
Acute retroviral syndrome, n (%)	42(86)	–	–
AHI administered ART before time of MRI, Mean(SD) days on ART before MRI	n = 23, 2(1.1)	–	–
CD4 cells/mm^3, Mean(SD)	421(234)	–	–
CD8 cells/mm^3, Mean(SD)	718(538)	–	–
CD4:CD8, Mean(SD)	0.8(0.5)	–	–
Plasma $\log_{10}$ HIV RNA, Mean (SD)	6.1(1.1)	–	–
Self-reported drug use in last 4 months, n (%)	9 (18)	–	–
NPZ-4, Mean(SD)[a]	0.2(0.8)	–	–

All P values were obtained with 2 sample t-tests or chi-squared tests for continuous and categorical variables, respectively.

[a] NPZ-4 available for 45 participants.

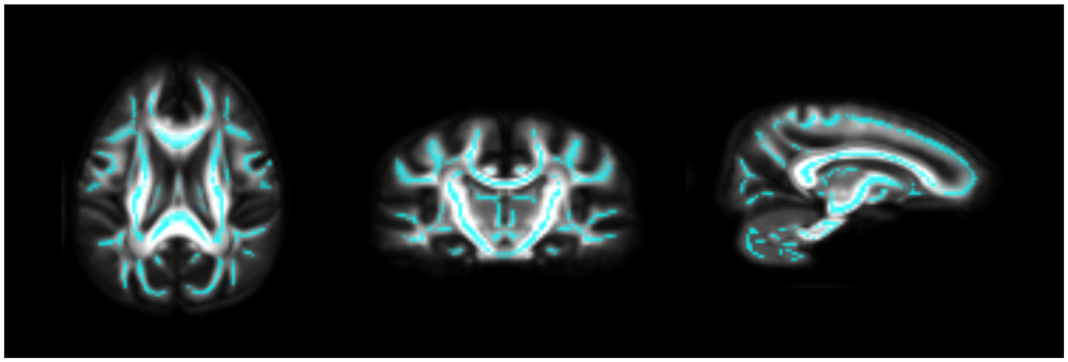

Fig. 1. No statistically different DTI indices between AHI and HIV uninfected controls: AHI exhibited no statistically significant differences in DTI metrics (FA, MD, RD, AD) compared to uninfected controls. Statistical map shown overlaid on tract based skeleton mask where comparisons were made in cyan (no voxels indicated $p < 0.05$, corrected for family wise error).

standardized checklist and completed by a physician. Participants grouped as Fiebig I/II had higher CD4:CD8 ratios [1.12(0.4) vs. 0.66(0.5)] and lower plasma $\log_{10}$ HIV RNA [5.53 (Heaton et al., 2004) vs. 6.3 (Heaton et al., 2004)] compared to participants in Fiebig III-V ($p < 0.05$). However, NPZ-4, CD4, and CD8 between Fiebig stages I/II and III-V did not reach significance ($p > 0.05$). The AHI group with brief exposure to ART had no differences in demographic or clinical variables compared to those without ART initiation (all $p > 0.05$) .

3.1. DTI

Examining all HIV infected participants as a group regardless of ART exposure, we found no statistically significant differences between AHI and controls in each of the DTI metrics (Fig. 1, FA, MD, RD, and AD). Specific ROIs chosen a priori also yielded no statistically significant differences between AHI and controls.

Diffusion indices were unrelated to HIV RNA, CD4 cell counts, CD8 cell counts, CD4:CD8 ratios or NPZ-4 (ART exposed and non-exposed) (all $p > 0.05$). Within the AHI group, ROIs included the superior longitudinal fasciculus, corona radiata, corpus callosum (total, genu, body, and splenium). ROI analyses revealed a modest elevation in the body of the corpus callosum in the ART exposed group compared to the unexposed group (Supplementary Fig. 2, $p = 0.046$).. Voxelwise analyses revealed higher FA and lower RD and MD bilaterally encompassing areas in the corpus callosum, corona radiata, and superior longitudinal fasciculus in the group with brief exposure to ART compared to those without (Supplemental Fig. 3,TFCE, $p_{FWE} < 0.05$).Fiebig analyses comparing early versus late groups resulted in small clusters of higher mean diffusivity in early versus late stages (Supplemental Fig. 4, TFCE, $p_{FWE} < 0.05$). ROIs were unrelated to Fiebig status in all DTI metrics (FA, MD, RD, AD, each $p > 0.05$).

3.2. rsFC

The group analysis revealed reduced functional connectivity between left parahippocampal cortex of the DMN and left middle frontal gyrus in the AHI group compared to controls (Table 2, Fig. 2, $p_{FWE} < 0.002$). There were no statistically significant group differences in rsFC for any other cortical or subcortical striatal network seeds. Within the AHI group, exposure to ART and Fiebig stage (early versus late) were unrelated to rsFC (each $p_{FWE} > 0.002$).

Regarding clinical variables in the AHI group, a higher baseline CD4 cell count was associated with increased, thus better, rsFC between right lateral parietal cortex of the DMN and left precuneus (Table 3, Fig. 3A, $p_{FWE} < 0.002$). Similarly, higher CD4 count was associated with greater rsFC between right parahippocampal cortex of the DMN and right inferior occipital gyrus (Table 3, Fig. 3B, $p_{FWE} < 0.002$). Better performance on the NPZ-4 was associated with greater rsFC between bilateral dorsal caudate and right inferior parietal lobule (Table 3, Fig. 3C, $p_{FWE} < 0.002$). There were no associations between rsFC and the other clinical variables, including HIV RNA, CD8 cell counts, or CD4:CD8 ratios.

4. Discussion

This study aimed to examine brain structure and functional connectivity in AHI compared to demographically similar uninfected controls. We identify relatively preserved brain integrity using DTI and rsFC in a group of AHI individuals compared to matched uninfected controls. Group comparisons identified no statistically significant differences between AHI and controls using quantitative white matter integrity measures. However, we found marginal but statistically significant better white matter integrity among participants who had a very brief exposure to ART compared those who were imaged just prior to starting ART. In contrast, AHI individuals exhibited reduced functional connectivity between the parahippocampal cortex of the DMN and the left middle frontal gyrus, with no differences by ART exposure. Overall, these results suggest largely preserved brain function and integrity during AHI and premise for the preservation of brain integrity during chronic HIV through early and persistent viral suppression with ART. Within AHI, higher CD4 count and neuropsychological performance was associated with increased rsFC of DMN and dorsal caudate network regions respectively.

Though there were no differences in DTI between AHI and controls in either voxelwise of ROI analyses, we did note differences by treatment status, even though treatment generally involved only a few doses of medications. In other acute and primary cohorts, Cao et al. report differences in the corpus callosum as early as 4 months of infection, with Wright et al. showing relatively preserved diffusion in primary HIV compared to uninfected controls (Cao et al., 2015; Wright et al., 2015). Our group wise analyses showed no differences by HIV status, however this may be reliant on DTI's sensitivity to detect nuanced changes in microstructure within only days to weeks after infection versus a differential sensitivity and earlier detection in resting state modalities. Future longitudinal studies would be better positioned to define microstructural abnormalities and establish a timeline of diffusion and resting state patterns from acute to primary to chronic HIV. Here, those with brief exposure to ART, exhibited higher FA and lower MD and RD in the callosum and regions of the corona radiata that suggest improved integrity (preserved directional flow and limited overall diffusion) for those on ART (Curran et al., 2016; Soares et al., 2013). These trends in those briefly exposed to treatment suggest that early neuropathogenic mechanisms operative within days of infection are moderated by ART. Though we do not hypothesize that very brief exposure to ART would significantly modulate DTI metrics, these comparisons were completed to ensure that the results were not significantly moderated by variability in treatment. Alternatively ART may directly drive these changes and therefore any causal model is

Table 2
Coordinates for cortical and subcortical networks used in resting-state analyses.[a]

Network	Seeds	Coordinates
Cortical networks		
Default mode network (DMN)[a]		
	Medial prefrontal cortex (mPFC)	1, 40, 19
	Posterior cingulate/retrosplenial cortex (PCC)	-1, −53, 25
	Left inferior parietal lobule (L IPL)	−45, −70, 24
	Right inferior parietal lobule (R IPL)	53, −68, 25
	Left hippocampal formation (L HF)	−23, −25, −16
	Right hippocampal formation (R HF)	23, −25, −16
	Left parahippocampal cortex (L PHC)	−25, −40, −14
	Right parahippocampal cortex (R PHC)	25, −40, −14
Fronto-parietal network (FPN)[b]		
	Left intraparietal sulcus (L IPS)	−31, −63, 42
	Right intraparietal sulcus (R IPS)	30, −65, 39
	Left dorsolateral prefrontal cortex (L dlPFC)	−43, 21, 38
	Right dorsolateral prefrontal cortex (R dlPFC)	43, 21, 38
Cingulo-opercular network (CON)[b]		
	Left anterior insula/frontal operculum (L aIfO)	−35, 14, 6
	Right anterior insula/frontal operculum (R aIfO)	36, 16, 5
	Dorsal anterior cingulate/mesial frontal cortex (dACC/msFC)	−1, 8, 50
Subcortical striatal networks[c]		
	Bilateral dorsal caudate (DC)	± 13, 15, 9
	Bilateral dorsal caudal putamen (DCP)	± 28, 1, 3
	Bilateral dorsal rostral putamen (DRP)	± 25, 8, 6
	Bilateral ventral rostral putamen (VRP)	± 20, 12, −3
	Bilateral ventral striatum inferior (VSi)	± 9, 9, −8
	Bilateral ventral striatum superior (VSs)	± 10, 15, 0

All seed ROIs are reported in Montreal Neurological Institute (MNI-152) template space.

[a] Default mode network seeds were selected from Andrews-Hanna et al., 2007.

[b] fronto-parietal and cingulo-opercular seeds were selected from Dosenback et al., 2007.

[c] subcortical striatal network seeds were selected from Di Martino et al., 2008.

speculative. AHI is also associated with a substantial host immune response and alterations in choline by MRS, implying the possibility that inflammation drives these measures (Valcour et al., 2012).

Reduced connectivity between the parahippocampal gyrus of the DMN and left middle frontal gyrus in AHI is consistent with a recent study showing diminished rsFC within the DMN using independent component analysis in treatment naïve individuals with early to chronic HIV (1–120 months after infection) (Zhuang et al., 2017). Similar

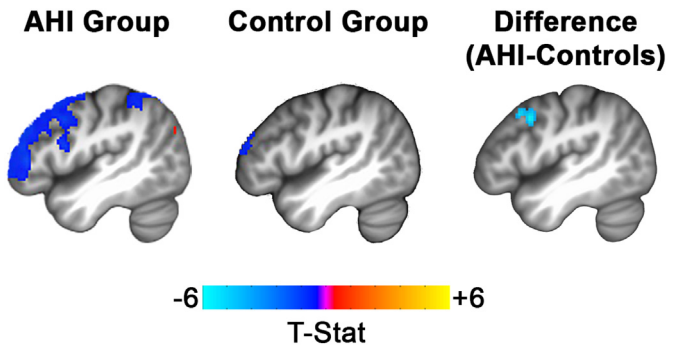

Fig. 2. Reduced rsFC in AHI versus uninfected controls.
AHI exhibited reduced rsFC between left parahippocampal cortex (L PHC) of the default mode network and left middle frontal gyrus. Images from left to right: L PHC rsFC for the AHI group; L PHC rsFC for the uninfected control group; Group difference map showing significantly reduced connectivity in AHI as compared with uninfected controls (AHI-Controls) ($p < 0.001$ uncorrected, pFWE < 0.002, *significant after Bonferroni-correction). Results are displayed on the group average structural MRI in MNI template space. Color bar indicates uncorrected *t* values.

Table 3
All regression results from resting-state analyses.

Seed ROI	Cluster location	MNI coordinates (x, y, z)	Cluster size (voxels)	t-value
AHI versus Controls				
L PHC	L. middle frontal gyrus overlapping with dlPFC	−49, 10, 40	187	−5.56
AHI only group where rsFC was associated with cd4 count				
R LatPar	L. precuneus	−19, −76, 24	519	6.02
R PHC	*R. inferior* occipital gyrus	35, −74, −10	518	5.50
AHI only group where rsFC was associated with NPZ-4				
B DC	R. inferior parietal lobule	41, −34, 32	214	4.89

All regression results were significant at the whole-brain level ($p_{FWE} = 0.002$, uncorrected $p = 0.001$, Bonferroni-corrected for number of seed ROIs). Abbreviations: L PHC = left parahippocampal cortex; DMN = default mode network; R LatPar = right lateral parietal cortex; R PHC = right parahippocampal cortex; B DC = bilateral dorsal caudate; L = left; R = right; dlPFC = dorsolateral prefrontal cortex; NPZ-4 = global neuropsychological performance measure.

reductions in rsFC of the DMN have also been reported in chronic HIV (Ortega et al., 2015; Thomas et al., 2013; Guha et al., 2016). Other studies using magnetoencephalography have also found reductions in beta oscillations of DMN regions at rest in older adults with chronic HIV (Becker et al., 2013). Our findings are also relevant to other studies in chronic HIV populations showing altered rsFC or integration between the DMN and the FPN, which includes the middle frontal gyrus (Thomas et al., 2013; Thomas et al., 2015). More broadly, the parahippocampal gyrus has been implicated as an entry site of varicella-zoster virus (Sarrazin et al., 2012). This common finding across neurovirulent viruses might raise the possibility of the parahippocampal gyrus serving as an early site of infection or entry point for HIV. Autopsy studies of individuals on ART at the time of death demonstrate substantial macrophage infiltration in these regions (Anthony et al., 2005). Prior work by members of our team revealed HIV viral RNA in the CSF within 8 days of infection and significant correlations between viral detection and elevated levels of central inflammation (Valcour et al., 2012; Sailasuta et al., 2012). The presence of the virus in the brain very soon after infection provides a neural substrate for altered brain integrity. rsFC is highly sensitive to these initial dynamics of neural injury, with microstructural and macrostructural abnormalities expected to occur subsequently in the absence, or despite, initiation of antiretroviral therapy. In the present study, reduced rsFC of the parahippocampal gyrus in AHI could be explained either by direct neuronal injury, by indirect neuronal dysfunction due to macrophage and microglial activation, by astrocyte dysfunction associated with the virus or due to a type 1 statistical error (due to the number of reported comparisons). Further longitudinal studies will be needed to investigate the relationship between this early minor dysfunction in rsFC in AHI and more extensive structural and functional imaging abnormalities identified in chronic HIV. Within the AHI group, we found that better global neuropsychological performance was associated with greater rsFC between dorsal caudate and right inferior parietal lobule. Our finding is relevant to a previous study revealing a similar relationship between neuropsychological performance and rsFC of a lateral occipital network which included the inferior parietal cortex using independent component analysis in individuals recently infected with HIV (~1 year of exposure) (Wang et al., 2011). The results are also consistent with a study showing a positive correlation neuropsychological performance and alpha activity in the postcentral gyrus in older adults with chronic HIV using magnetoencephalography (Wilson et al., 2015). Together, these results suggest that alterations in large scale network connectivity, in particular decreased rsFC with inferior parietal cortex, may be a marker of impaired cognitive performance in chronic HIV.

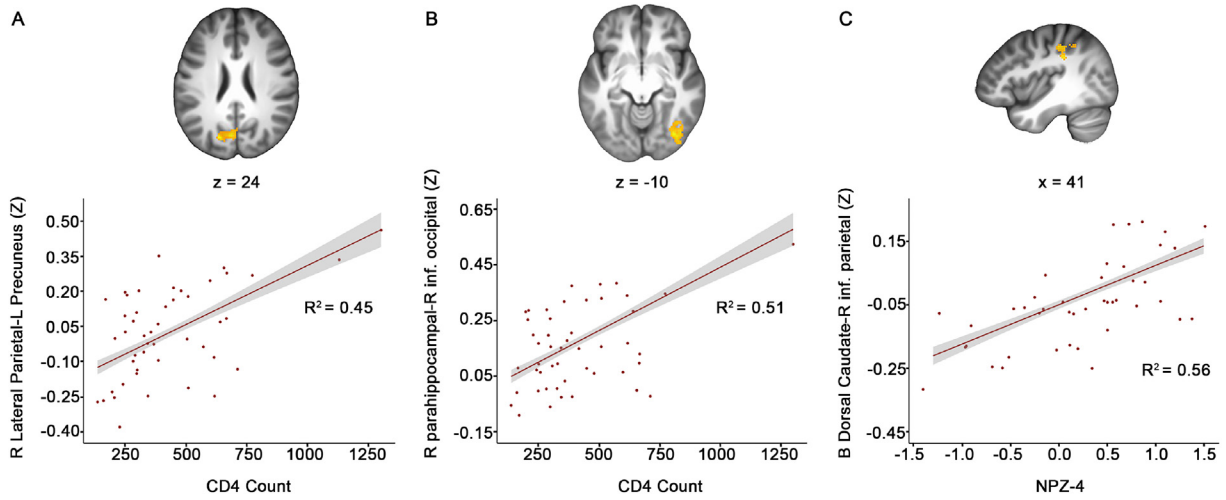

Fig. 3. Blood biomarkers and neuropsychological performance associate with rsFC in AHI.
A. *Top,* Greater rsFC between right lateral parietal seed and left precuneus associated with greater CD4 counts; *Bottom*, scatterplot shows the relationship between right lateral parietal-left precuneus connectivity values and CD4 count. B. *Top*, Greater rsFC between right parahippocampal seed and right inferior occipital gyrus associated with greater CD4 count; *Bottom*, scatterplot shows the relationship between right parahippocampal-right inferior occipital connectivity values and CD4 count. C. *Top*, Greater rsFC between the bilateral dorsal caudate seed and right inferior parietal lobe associated with greater NPZ-4 global scores; *Bottom*, scatterplot shows the relationship between bilateral dorsal caudate-right inferior parietal connectivity values and NPZ-4 global scores. $p < 0.001$ uncorrected, $p_{FWE} < 0.002$, *significant after Bonferroni-correction. Results are displayed on the group average structural MRI in MNI template space.

A few limitations merit discussion. Longitudinal data may offer the best approach to best elucidate changes that occur during the course of initial HIV transmission. Our cross-sectional data serve as a foundation for these studies and highlight one limitation to the present work. Additionally, while randomizing AHI participants to ART would have would further described the CNS impact of treatment in AHI, this was not possible, as early ART can reduce the size of the latent viral reservoir and withholding treatment is not consistent with current treatment guidelines (Ananworanich et al., 2012). Although the majority of all participants were male, sex differences were not adjusted due to unbalanced proportions of females to males between AHI and the control group. Sensitivity analyses were completed to determine whether the pattern of results were maintained after restricting cases to male participants. No differences in outcomes were observed for the DTI comparisons. The resting state outcomes mirrored the results based on the full sample, though the effect was reduced.. Despite the strengths, we also recognize the limitations inherent in using atlas based registration approaches for neuroimaging analyses. In addition, image processing techniques and post processing steps may influence detectability of subtle differences. We attempted to mitigate these effects by using validated approaches by prior investigators. High-dimensional normalization using the full tensor features was employed to help improve alignment of white matter tracts and reduce confounding effects of shape differences (Zhang et al., 2007a). For the present study, we focused on rsFC for nine cortical and subcortical networks that have previously been implicated in HIV (Wang et al., 2011; Ipser et al., 2015; Ortega et al., 2015; Thomas et al., 2013; Zhuang et al., 2017; Thomas et al., 2015). However, future resting-state fMRI studies using data-driven approaches, such as independent component analysis, will be necessary to determine whether rsFC is altered in other resting-state networks in acute HIV.

We must also consider the possibility that the analyses were limited by a small sample size, despite this report including a substantial number of people with AHI compared to the published literature. Few studies provided consensus on neuroimaging signatures in initial HIV disease, with a gap in knowledge regarding brain integrity in AHI during the earliest stages of infection. In this critical stage after HIV infection and optimal treatment was administered, our multimodal MRI analyses reflected absence of widespread abnormalities between AHI and controls indicating relatively preserved brain integrity. The lack of substantial findings is further supported by prior reports that large structural changes and CSF neurofilament light chain abnormalities are not found during this stage (Peluso et al., 2015). Instead, our findings illustrate only subtle differences in white matter diffusion and rsFC. Further longitudinal studies are warranted to explore the evolution of brain injury despite maximal treatment and determine if early ART is sufficient to prevent brain dysfunction.

Acknowledgements

This work was supported by National Institutes of Health grants R01MH113560 (VV and RP), K24MH098759 (VV), R01MH095613 (VV and SS), R01NS084911 (JA and SS) and a cooperative agreement (W81XWH-07-2-0067) between the Henry M. Jackson Foundation for the Advancement of Military Medicine, Inc., and the U.S. Department of Defense (DoD) with supplemental funding from the National Institute of Mental Health. We thank our study participants and the Government Pharmaceutical Organization, Thailand (GPO), ViiV Healthcare, Gilead and Merck for providing the antiretroviral medications for this study.

Appendix A. Supplementary data

Supplementary data to this article can be found online at https://doi.org/10.1016/j.nicl.2018.07.024.

References

Ananworanich, J., Schuetz, A., Vandergeeten, C., et al., 2012. Impact of multi-targeted antiretroviral treatment on Gut T cell depletion and HIV reservoir seeding during acute HIV infection. In: Emery, S. (Ed.), PLoS One. 7 (3), e33948. https://doi.org/10.1371/journal.pone.0033948.

Ananworanich, J., Chomont, N., Eller, L.A., et al., 2016. HIV DNA set point is rapidly established in acute HIV infection and dramatically reduced by early ART. EBioMedicine 11, 68–72. https://doi.org/10.1016/j.ebiom.2016.07.024.

Ances, B.M., Ortega, M., Vaida, F., Heaps, J., Paul, R., 2012. Independent effects of HIV, aging, and HAART on brain volumetric measures. J. Acquir. Immune Defic. Syndr. 59 (5), 469–477. https://doi.org/10.1097/QAI.0b013e318249db17.

Andrews-Hanna, J.R., Snyder, A.Z., Vincent, J.L., Lustig, C., Head, D., Raichle, M.E., Buckner, R.L., 2007. Disruption of large-scale brain systems in advanced aging. Neuron 56, 924–935.

Andrews-Hanna, J.R., Reidler, J.S., Sepulcre, J., Poulin, R., Buckner, R.L., 2010. Functional-anatomic fractionation of the brain's default network. Neuron 65 (4), 550–562. https://doi.org/10.1016/j.neuron.2010.02.005.

Anthony, I.C., Ramage, S.N., Carnie, F.W., Simmonds, P., Bell, J.E., 2005. Influence of HAART on HIV-related CNS disease and Neuroinflammation. J. Neuropathol. Exp. Neurol. 64 (6), 529–536. https://doi.org/10.1093/jnen/64.6.529.

Becker, K.M., Heinrichs-Graham, E., Fox, H.S., et al., 2013. Decreased MEG beta oscillations in HIV-infected older adults during the resting state. J. Neuro-Oncol. 19 (6), 586–594. https://doi.org/10.1007/s13365-013-0220-8.

Biswal, B., Yetkin, F.Z., Haughton, V.M., Hyde, J.S., 1995. Functional connectivity in the motor cortex of resting human brain using echo-planar MRI. Magn. Reson. Med. 34 (4), 537–541. http://www.ncbi.nlm.nih.gov/pubmed/8524021, Accessed date: 7 February 2018.

Cao, B., Kong, X., Kettering, C., Yu, P., Ragin, A., 2015. Determinants of HIV-induced brain changes in three different periods of the early clinical course: a data mining analysis. NeuroImage Clin. 9, 75–82. https://doi.org/10.1016/j.nicl.2015.07.012.

Carp, J., Peelle, J.E., Duff, E., 2012. On the Plurality of (Methodological) Worlds: Estimating the Analytic Flexibility of fMRI Experiments. https://doi.org/10.3389/fnins.2012.00149.

Ciric, R., Wolf, D.H., Power, J.D., et al., 2017. Benchmarking of participant-level confound regression strategies for the control of motion artifact in studies of functional connectivity. NeuroImage 154, 174–187. https://doi.org/10.1016/J.NEUROIMAGE.2017.03.020.

Cox, R.W., 1996. AFNI: software for analysis and visualization of functional magnetic resonance neuroimages. Comput. Biomed. Res. 29 (3), 162–173. http://www.ncbi.nlm.nih.gov/pubmed/8812068, Accessed date: 8 February 2018.

Curran, K.M., Emsell, L., Leemans, A., Curran, K.M., Emsell, L., Leemans, A., 2016. Quantitative DTI Measures Why is Quantification Important in Medical Imaging? https://doi.org/10.1007/978-1-4939-3118-7_5.

De Souza, M.S., Phanuphak, N., Pinyakorn, S., et al., 2015. Impact of nucleic acid testing relative to antigen/antibody combination immunoassay on the detection of acute HIV infection. AIDS 29 (7), 793–800. https://doi.org/10.1097/QAD.0000000000000616.

Di Martino, A., Scheres, A., Margulies, D.S., et al., 2008. Functional connectivity of human striatum: a resting state fMRI study. Cereb. Cortex 18 (12), 2735–2747. https://doi.org/10.1093/cercor/bhn041.

Dosenbach, N.U.F., Fair, D.A., Miezin, F.M., Cohen, A.L., Wenger, K.K., Dosenbach, R.A.T., Fox, M.D., Snyder, A.Z., Vincent, J.L., Raichle, M.E., Schlaggar, B.L., Petersen, S.E., 2007. Distinct brain networks for adaptive and stable task control in humans. Proceedings of the National Academy of Sciences USA 104, 11073–11078.

Eklund, A., Nichols, T.E., Knutsson, H., 2016. Cluster failure: why fMRI inferences for spatial extent have inflated false-positive rates. Proc. Natl. Acad. Sci. U. S. A. 113 (28), 7900–7905. https://doi.org/10.1073/pnas.1602413113.

Fiebig, E.W., Wright, D.J., Rawal, B.D., et al., 2003. Dynamics of HIV viremia and antibody seroconversion in plasma donors: implications for diagnosis and staging of primary HIV infection. AIDS 17 (13), 1871–1879. https://doi.org/10.1097/01.aids.0000076308.76477.b8.

Filippi, C.G., Ulug, A.M., Ryan, E., Ferrando, S.J., van Gorp, W., 2001. Diffusion tensor imaging of patients with HIV and normal-appearing white matter on MR images of the brain. AJNR Am. J. Neuroradiol. 22 (2), 277–283. http://www.ncbi.nlm.nih.gov/pubmed/11156769, Accessed date: 7 March 2017.

Forman, S.D., Cohen, J.D., Fitzgerald, M., Eddy, W.F., Mintun, M.A., Noll, D.C., 1995. Improved assessment of significant activation in functional magnetic resonance imaging (fMRI): use of a cluster-size threshold. Magn. Reson. Med. 33 (5), 636–647. http://www.ncbi.nlm.nih.gov/pubmed/7596267, Accessed date: 7 February 2018.

Garyfallidis, E., Brett, M., Amirbekian, B., et al., 2014. Dipy, a library for the analysis of diffusion MRI data. Front. Neuroinform. 8, 8. https://doi.org/10.3389/fninf.2014.00008.

Gongvatana, A., Schweinsburg, B.C., Taylor, M.J., et al., 2009. White matter tract injury and cognitive impairment in human immunodeficiency virus-infected individuals. J. Neuro-Oncol. 15 (2), 187–195. https://doi.org/10.1080/13550280902769756.

Guha, A., Wang, L., Tanenbaum, A., et al., 2016. Intrinsic network connectivity abnormalities in HIV-infected individuals over age 60. J. Neuro-Oncol. 22 (1), 80–87. https://doi.org/10.1007/s13365-015-0370-y.

Hakkers, C.S., Arends, J.E., Barth, R.E., Du Plessis, S., Hoepelman, A.I.M., Vink, M., 2017. Review of functional MRI in HIV: effects of aging and medication. J. Neuro-Oncol. 23 (1), 20–32. https://doi.org/10.1007/s13365-016-0483-y.

Heaton, R.K., Marcotte, T.D., Mindt, M.R., et al., 2004. The impact of HIV-associated neuropsychological impairment on everyday functioning. J. Int. Neuropsychol. Soc. 10 (3), 317–331. https://doi.org/10.1017/S1355617704102130.

Heaton, R.K., Clifford, D.B., Franklin, D.R., et al., 2010. HIV-associated neurocognitive disorders persist in the era of potent antiretroviral therapy: CHARTER study. Neurology 75 (23), 2087–2096. https://doi.org/10.1212/WNL.0b013e318200d727.

Hellmuth, J., Fletcher, J.L.K., Valcour, V., et al., 2016. Neurologic signs and symptoms frequently manifest in acute HIV infection. Neurology 87 (2), 148–154. https://doi.org/10.1212/WNL.0000000000002837.

Ipser, J.C., Brown, G.G., Bischoff-Grethe, A., et al., 2015. HIV infection is associated with attenuated Frontostriatal intrinsic connectivity: a preliminary study. J. Int. Neuropsychol. Soc. 21 (3), 203–213. https://doi.org/10.1017/S1355617715000156.

Jenkinson, M., Bannister, P., Brady, M., Smith, S., 2002. Improved optimization for the robust and accurate linear registration and motion correction of brain images. NeuroImage 17 (2), 825–841. http://www.ncbi.nlm.nih.gov/pubmed/12377157, Accessed date: 7 February 2018.

Jernigan, T.L., Archibald, S.L., Fennema-Notestine, C., et al., 2011. Clinical factors related to brain structure in HIV: the CHARTER study. J. Neuro-Oncol. 17 (3), 248–257. https://doi.org/10.1007/s13365-011-0032-7.

Kore, I., Ananworanich, J., Valcour, V., et al., 2015. Neuropsychological impairment in acute HIV and the effect of immediate antiretroviral therapy. J. Acquir. Immune Defic. Syndr. 70 (4), 393–399. https://doi.org/10.1097/QAI.0000000000000746.

Lavreys, L., Baeten, J.M., Chohan, V., et al., 2006. Higher set point plasma viral load and more-severe acute HIV type 1 (HIV-1) illness predict mortality among high-risk HIV-1-infected African women. Clin. Infect. Dis. 42 (9), 1333–1339. https://doi.org/10.1086/503258.

Maldjian, J.A., Laurienti, P.J., Kraft, R.A., Burdette, J.H., 2003. An automated method for neuroanatomic and cytoarchitectonic atlas-based interrogation of fMRI data sets. NeuroImage 19 (3), 1233–1239. http://www.ncbi.nlm.nih.gov/pubmed/12880848, Accessed date: 7 February 2018.

O'Connor, E.E., Zeffiro, T.A., Zeffiro, T.A., 2018. Brain structural changes following HIV infection: meta-analysis. AJNR Am. J. Neuroradiol. 39 (1), 54–62. https://doi.org/10.3174/ajnr.A5432.

Ortega, M., Brier, M.R., Ances, B.M., 2015. Effects of HIV and combination antiretroviral therapy on cortico-striatal functional connectivity. AIDS 29 (6), 703–712. https://doi.org/10.1097/QAD.0000000000000611.

Peluso, M.J., Valcour, V., Ananworanich, J., et al., 2015. Absence of cerebrospinal fluid signs of neuronal injury before and after immediate antiretroviral therapy in acute HIV infection. J. Infect. Dis. 212 (11), 1759–1767. https://doi.org/10.1093/infdis/jiv296.

Philippi, C.L., Motzkin, J.C., Pujara, M.S., Koenigs, M., 2015. Subclinical depression severity is associated with distinct patterns of functional connectivity for subregions of anterior cingulate cortex. Journal of Psychiatric Research 71, 103–111.

Pierpaoli, C., Basser, P.J., 1996. Toward a quantitative assessment of diffusion anisotropy. Magn. Reson. Med. 36 (6), 893–906. https://doi.org/10.1002/mrm.1910360612.

Power, J.D., Barnes, K.A., Snyder, A.Z., Schlaggar, B.L., Petersen, S.E., 2012. Spurious but systematic correlations in functional connectivity MRI networks arise from subject motion. NeuroImage 59 (3), 2142–2154. https://doi.org/10.1016/j.neuroimage.2011.10.018.

Power, J.D., Mitra, A., Laumann, T.O., Snyder, A.Z., Schlaggar, B.L., Petersen, S.E., 2014. Methods to detect, characterize, and remove motion artifact in resting state fMRI. NeuroImage 84, 320–341. https://doi.org/10.1016/j.neuroimage.2013.08.048.

Price, R.W., Spudich, S., 2008. Antiretroviral therapy and central nervous system HIV type 1 infection. J. Infect. Dis. 197 (s3), S294–S306. https://doi.org/10.1086/533419.

Ragin, A.B., Wu, Y., Gao, Y., et al., 2015. Brain alterations within the first 100 days of HIV infection. Ann. Clin. Transl Neurol. 2 (1), 12–21. https://doi.org/10.1002/acn3.136.

Sailasuta, N., Ross, W., Ananworanich, J., et al., 2012. Change in brain magnetic resonance spectroscopy after treatment during acute HIV infection. PLoS One 7 (11), e49272. https://doi.org/10.1371/journal.pone.0049272.

Sarrazin, J.-L., Bonneville, F., Martin-Blondel, G., 2012. Brain infections. Diagn. Interv. Imaging 93, 473–490. https://doi.org/10.1016/j.diii.2012.04.020.

Satterthwaite, T.D., Elliott, M.A., Gerraty, R.T., et al., 2013. An improved framework for confound regression and filtering for control of motion artifact in the preprocessing of resting-state functional connectivity data. NeuroImage 64, 240–256. https://doi.org/10.1016/j.neuroimage.2012.08.052.

Sidtis, J.J., Gatsonis, C., Price, R.W., et al., 1993. Zidovudine treatment of the AIDS dementia complex: results of a placebo-controlled trial. AIDS Clinical Trials Group. Ann. Neurol. 33 (4), 343–349. https://doi.org/10.1002/ana.410330403.

Smith, S.M., Jenkinson, M., Johansen-Berg, H., et al., 2006. Tract-based spatial statistics: voxelwise analysis of multi-subject diffusion data. NeuroImage 31 (4), 1487–1505. https://doi.org/10.1016/j.neuroimage.2006.02.024.

Soares, J.M., Marques, P., Alves, V., Sousa, N., 2013. A hitchhiker's guide to diffusion tensor imaging. Front. Neurosci. 7, 31. https://doi.org/10.3389/fnins.2013.00031.

Stebbins, G.T., Smith, C.A., Bartt, R.E., et al., 2007. HIV-associated alterations in normal-appearing white matter: a voxel-wise diffusion tensor imaging study. J. Acquir. Immune Defic. Syndr. 46 (5), 564–573. http://www.ncbi.nlm.nih.gov/pubmed/18193498, Accessed date: 25 February 2018.

Su, T., Caan, M.W.A., Wit, F.W.N.M., et al., 2016. White matter structure alterations in HIV-1-infected men with sustained suppression of viraemia on treatment on behalf of the AGE h IV cohort study. AIDS. https://doi.org/10.1097/QAD.0000000000000945.

Thomas, J.B., Brier, M.R., Snyder, A.Z., Vaida, F.F., Ances, B.M., 2013. Pathways to neurodegeneration: effects of HIV and aging on resting-state functional connectivity. Neurology 80 (13), 1186–1193. https://doi.org/10.1212/WNL.0b013e318288792b.

Thomas, J.B., Brier, M.R., Ortega, M., Benzinger, T.L., Ances, B.M., 2015. Weighted brain networks in disease: centrality and entropy in human immunodeficiency virus and aging. Neurobiol. Aging 36 (1), 401–412. https://doi.org/10.1016/j.neurobiolaging.2014.06.019.

Underwood, J., Cole, J.H., Caan, M., et al., 2017. Gray and white matter abnormalities in treated human immunodeficiency virus disease and their relationship to cognitive function. Clin. Infect. Dis. 65 (3), 422–432. https://doi.org/10.1093/cid/cix301.

Valcour, V., Chalermchai, T., Sailasuta, N., et al., 2012. Central nervous system viral invasion and inflammation during acute HIV infection. J. Infect. Dis. 206 (2), 275–282. https://doi.org/10.1093/infdis/jis326.

Wang, X., Foryt, P., Ochs, R., et al., 2011. Abnormalities in resting-state functional connectivity in early human immunodeficiency virus infection. Brain Connect. 1 (3), 207–217. https://doi.org/10.1089/brain.2011.0016.

Watkins, C.C., Treisman, G.J., 2015. Cognitive impairment in patients with AIDS - prevalence and severity. HIV AIDS (Auckl) 7, 35–47. https://doi.org/10.2147/HIV.S39665.

Wendelken, L.A., Jahanshad, N., Rosen, H.J., et al., 2016. ApoE ε4 is associated with cognition, brain integrity, and atrophy in HIV over age 60. J. Acquir. Immune Defic. Syndr. 73 (4), 426–432. https://doi.org/10.1097/QAI.0000000000001091.

Wilson, T.W., Heinrichs-Graham, E., Becker, K.M., et al., 2015. Multimodal neuroimaging evidence of alterations in cortical structure and function in HIV-infected older adults. Hum. Brain Mapp. 36 (3), 897–910. https://doi.org/10.1002/hbm.22674.

Winkler, A.M., Ridgway, G.R., Webster, M.A., Smith, S.M., Nichols, T.E., 2014. Permutation inference for the general linear model. NeuroImage 92, 381–397.

https://doi.org/10.1016/j.neuroimage.2014.01.060.
Woods, S.P., Moore, D.J., Weber, E., Grant, I., 2009. Cognitive neuropsychology of HIV-associated neurocognitive disorders. Neuropsychol. Rev. 19 (2), 152–168. https://doi.org/10.1007/s11065-009-9102-5.
Wright, P.W., Fernández, R.J., VFF, 2015. Cerebral white matter integrity during primary HIV infection. AIDS 29 (4), 433–442. https://doi.org/10.1097/QAD.0000000000000560.
Yan, C.-G., Craddock, R.C., He, Y., Milham, M.P., 2013. Addressing head motion dependencies for small-world topologies in functional connectomics. Front. Hum. Neurosci. 7, 910. https://doi.org/10.3389/fnhum.2013.00910.
Zhang, Y., Brady, M., Smith, S., 2001. Segmentation of brain MR images through a hidden Markov random field model and the expectation-maximization algorithm. IEEE Trans. Med. Imaging 20 (1), 45–57. https://doi.org/10.1109/42.906424.
Zhang, Hui, Avants, B.B., Yushkevich, P.A., et al., 2007a. High-dimensional spatial normalization of diffusion tensor images improves the detection of white matter differences: an example study using amyotrophic lateral sclerosis. IEEE Trans. Med. Imaging 26 (11), 1585–1597. https://doi.org/10.1109/TMI.2007.906784.
Zhang, H., Yushkevich, P.A., Rueckert, D., Gee, J.C., 2007b. Unbiased white matter atlas construction using diffusion tensor images. In: Medical Image Computing and Computer-Assisted Intervention – MICCAI. 2007. Springer Berlin Heidelberg, Berlin, Heidelberg, pp. 211–218. https://doi.org/10.1007/978-3-540-75759-7_26.
Zhuang, Y., Qiu, X., Wang, L., et al., 2017. Combination antiretroviral therapy improves cognitive performance and functional connectivity in treatment-naïve HIV-infected individuals. J. Neuro-Oncol. 23 (5), 704–712. https://doi.org/10.1007/s13365-017-0553-9.